European Journal of Pharmaceutics and Biopharmaceutics 73 (2009) 179–186

Contents lists available at ScienceDirect

European Journal of Pharmaceutics and Biopharmaceutics

journal homepage: www.elsevier.com/locate/ejpb

Research paper

Quantification of microparticle coating quality by confocal laser scanning microscopy (CLSM)

F. Depypere [a,*], P. Van Oostveldt [b], J.G. Pieters [c], K. Dewettinck [a]

[a] Laboratory of Food Technology and Engineering, Ghent University, Gent, Belgium
[b] Laboratory of Biochemistry and Molecular Cytology, Ghent University, Gent, Belgium
[c] Biosystems Engineering, Ghent University, Gent, Belgium

ARTICLE INFO

Article history:
Received 24 April 2008
Accepted in revised form 20 April 2009
Available online 3 May 2009

Keywords:
Coating quality
Coating thickness
Quantification
Confocal
Microscopy
CLSM
Microparticle
Fluid bed
Spray-drying

ABSTRACT

In this work, a novel protocol was developed for determining film coating thickness and coating quality of microparticles, based on the use of confocal laser scanning microscopy (CLSM). CLSM was found to be an adequate non-destructive technique for the quantification of the coating thickness and coating quality of individual thin-coated small particles. Combined with image analysis, it was possible to derive with high accuracy the coating thickness distribution of a representative number of microparticles. The performance of the novel methodology was assessed by the quantification of the coating thickness and coating quality of protein-coated microparticles produced by fluidized bed coating. It was found that the CLSM data on coating layer thickness were generally in good agreement with the results from chemical analysis, down to a thickness of 1–1.5 μm. Using CLSM the importance of setting up the appropriate distance between the coating nozzle and the powder bed with respect to microparticle coating quality in fluidized bed processing was illustrated. Coating quality was found to decrease with increasing distance the coating droplets have to travel before impinging onto the core particles as a result of spray-drying of the coating droplets. Also, coating quality decreased with increasing viscosity of the coating droplets, resulting in reduced spreading on the cores.

1. Introduction

Microencapsulation is a process in which a pure active ingredient or a mixture is coated with or entrapped within a protecting material or system. As a result, useful and otherwise unusual properties may be conferred to the microencapsulated ingredient, or unuseful properties may be eliminated from the original ingredient [1,2]. The performance of the end products of a particle coating microencapsulation process essentially depends on quality aspects such as microparticle film coating thickness, quality and morphology.

Better control of the particle coating microencapsulation process has therefore stimulated the efforts to monitor the coating process by measuring the coating thickness. Whereas a too thin coating will fail in its required performance (protection, controlled release, etc.), a too thick coating will result in delayed liberation, increased coating process times and hence, increasing costs [3].

A basic technique, commonly applied for tablets, to determine the endpoint of a coating process is taking samples in-process, weighing a known sample size and determining the theoretical amount of coating added [4]. First of all, this information assumes equal coating thickness around the complete tablet surface and between different tablets. Secondly, it is clear that for microparticles (100–500 μm), this technique has practical limitations.

The applicability of microscopic techniques such as SEM and conventional fluorescence microscopy is restricted to the sample surface. Therefore, in order to be able to study the coating layer around tablets or microparticles, these have to be sliced into two or more sections. As a result, this procedure is characterized by a high number of possible practical problems and artefacts. Conventionally, pellets are sliced into two sections and imaged by SEM or fluorescence microscopy [5–7]. Tedious protocols are reported to assure that pellets are cut in the equatorial plane [8]. For mechanical sectioning of smaller microparticles, it is clear that it is even more difficult to control the slicing plane.

Atomic force microscopy (AFM) studies microparticle surface roughness by using a sharp probe, moving over the sample surface in a raster scan [9]. From the detected deflections, a map of surface topography is generated [10]. AFM has the advantage of offering a better resolution (submicron range) than electron microscopy (EM) and is capable of non-destructively characterising non-conducting

* Corresponding author. Ghent University, Faculty of Bioscience Engineering, Department of Food Safety and Food Quality, Laboratory of Food Technology and Engineering (FTE), Coupure links 653, 9000 Gent, Belgium. Tel.: +32 9 264 61 67; fax: +32 9 264 62 18.
E-mail address: Frederic.Depypere@UGent.be (F. Depypere).

0939-6411/$ - see front matter © 2009 Elsevier B.V. All rights reserved.
doi:10.1016/j.ejpb.2009.04.007

surfaces [11]. Main limitations of AFM are thermal fluctuations and the finite size of the probe tip [12].

Also, near-IR spectra can be used in the prediction of film coating thickness as spectral changes occur when the coating thickness varies [4]. The range of film thicknesses investigated using this method, however, varies from 25 to 75 μm. These are rather large values, characteristic of the pharmaceutical industry, but considerably exceeding the thickness of a conventional food ingredient coating (5–10 μm) obtained via, e.g., a fluidized bed coating technique. Hence, near-IR spectroscopy does not assure the required spatial resolution [13].

Laser-induced breakdown spectroscopy (LIBS) is an elemental analysis technique well-suited to quickly study the microparticle surface and the internal component distribution, with minimal sample preparation, but suffers from the same drawback as for near-IR spectroscopy as the sampling size is approximately 500 μm in diameter [14] and the depth penetration per laser pulse is in the order of 10 μm. Nevertheless, for larger tablets, LIBS has the potential to provide both a rapid at-line analysis of multiple samples and the spatial resolution necessary for intra-tablet coating uniformity determination [13].

The above-described limitations associated with the mechanical sectioning of the microparticles can be overcome through the use of confocal laser scanning microscopy (CLSM). In this method, the operator is allowed to optically section the microparticle at any desired plane [8]. Andersson et al. [6] ascribed to the use of fluorescence microscopy the advantage that the core and the coat could be distinguished based on a difference in fluorescence intensity. However, Ruotsalainen et al. [15] showed that CLSM was even more powerful in studying the film–core interface. In their work, only the coating was fluorescently labelled and, hence, visualized by CLSM.

The potential for using CLSM as a non-destructive and convenient method for the study of microcapsules is very high [16]. This was concluded from CLSM's ability to adequately visualize the different components of alginate–polylysine–alginate microcapsules [17]. Furthermore, CLSM combined with computational image analysis allowed the quantitative determination of the thickness and composition of the wall material of microcapsules, prepared by complex coacervation [18]. Another study, by Lamprecht et al. [19] showed that with CLSM, it was possible to quickly determine the location as well as the amount of an encapsulated oil phase. Quantification of the CLSM images was facilitated by the spherical shape of both the encapsulated oil phase and the microcapsules themselves. Zimmermann et al. [20] used CLSM to validate a preparation technique for alginate microcapsules. It was concluded that CLSM allowed routine evaluation of capsule performance.

In a study on microparticles obtained after spray-drying, Lamprecht et al. [8] observed that the small size of the particles appeared to reach the limit of the resolution attainable with CLSM. It was indicated that a meaningful image resolution for particles smaller than 5 μm would be difficult to obtain. Nevertheless, CLSM was acknowledged as a very powerful technique for the characterization of microparticles, providing more information than any other microscopic inspection method. More recently, confocal micrographs of polyelectrolyte microcapsules in the size range of 2–5 μm have been recorded and first attempts have been made to derive the shell thickness of 5 μm sized microcapsules [21–23].

The considerable amount of literature cited above has one important thing in common with respect to the assessment of the microparticle quality, i.e., their focus is on either the coating surface or the average coating thickness. However, obtaining an average value for coating thickness alone does not adequately characterize a batch of coated microparticles; equally important are overall coating quality, inter- and intra-particle coating variability and the presence of coating deficiencies. Furthermore, one of the key goals of every batch microparticle coating process is to produce, batch by batch, uniform product quality and morphology, so coating quality also needs to be verified for different batches. In all of the above-mentioned studies, only the average coating thickness is estimated, while no information on the heterogeneity between individual microparticles is given. An exception is the work of Andersson et al. [6] who performed an analysis of film coating thickness of pharmaceutical pellets. In their work, each pellet was already characterized by a population of coating thicknesses rather than by one single value. However, mechanical sectioning of the spherical pellets was necessary in order to study the pellets under the fluorescence microscope.

None of the above cited studies presented a non-destructive quantification of coating quality of microparticles (about 250 μm) with very thin (~5 μm) coatings. Therefore, the objective of this work was to develop a novel protocol for determining film coating thickness and quality of microparticles, based on the use of confocal laser scanning microscopy. The performance of the novel methodology will be assessed by the quantification of the coating thickness and quality of microparticles produced by fluidized bed coating.

2. Materials and methods

2.1. Microparticle production

Fluidization experiments were performed in a laboratory-scale Glatt GPCG-1 fluidized bed (Glatt GmbH, Germany) comprising a tapered stainless steel (0.56 m height, 8.1° inclination) vessel with a stainless steel woven-wire mesh distributor at the base (0.14 m diameter). More information on the equipment can be found elsewhere [24,25]. Both the top-spray and bottom-spray configuration [2,26–29] were applied to coat glass beads Microbeads® (Sovitec, Belgium) with an average particle diameter of 204 μm. Two different proteins were selected as coating materials: aqueous solutions of 5–10 wt% sodium caseinate (Armor Protein, France) and gelatine ASF/A (Rousselot, Belgium), which is a porcine collagen hydrolysate, were prepared. In each case, the protein was dissolved into demineralised water, which was previously stained with 3 ppm Rhodamine B (99+%) (Across Organics, Belgium). In all experiments, 750 g of core particles were processed in a Glatt GPCG-1 fluidized bed. The inlet air was heated to 75 °C and a flow rate of 97 m^3/h or 55 m^3/h, resulting in good fluidization conditions in the top-spray and bottom-spray configuration, respectively, was selected. A binary nozzle was used to atomize the aqueous coating solution (room temperature) onto the fluidized particles. The nozzle atomization pressure was set at 3 bar in order to obtain sufficiently small coating droplets.

2.2. Coating thickness calculation

The theoretical coating thickness can be calculated based on the fact that a known amount of coating dry matter, M_c, is added to a fluidized powder mass, M_p. All core particles are considered to be spherical and to have an equal particle radius, r_p. Under the assumptions that no coating losses occur and that a coated particle can be considered as two concentric spheres, a theoretical reference value for coating thickness, d_c, can be found as (after [30])

$$d_c = r_p \cdot \left(\left(1 + \frac{\rho_p \cdot M_c}{\rho_c \cdot M_p} \right)^{1/3} - 1 \right) \quad (1)$$

where ρ_p is the particle density of the core particles (kg/m^3) and ρ_c is the particle density of the coating material (kg/m^3). The particle density of the core particles and the coating materials were obtained through toluene pycnometry. The particle density of the

glass beads was found to be 2467 ± 3 kg/m^3 while the particle density of the coating material was 944 ± 15 kg/m^3 and 1075 ± 11 kg/m^3 for sodium caseinate and gelatine hydrolysate, respectively.

Secondly, also the actual protein content of the coated microparticles was determined using the Lowry method [31–33]. This value for actual protein content was introduced in Eq. (1) as an estimate of M_c/M_p, and consequently, an experimental reference value for coating thickness was obtained. In contrast to the theoretical reference value, coating losses, e.g., through spray-drying of the coating solution, are included in the experimental reference value for coating layer thickness.

2.3. CLSM protocol

A Bio-Rad Radiance 2000 confocal laser scanning microscopy system (Bio-Rad, United Kingdom), attached to a Nikon Eclipse TE300 inverted fluorescence (Bio-Rad, UK) microscope, equipped with a He/Ne-laser with a laser power of 1.4 mW, generating a green excitation line of 543 nm, was used. Rhodamine B was detected on a photomultiplier using a HQ590/70 filter. All confocal images were taken with a Nikon S Fluor 40× objective (oil immersion, NA 1.30). All settings for the confocal microscope and the imaging of the microparticles were computer controlled through the software Lasersharp 2000 version 5.2 (Bio-Rad, UK). The following settings were kept constant during all experiments: laser power (20% of the maximum power), scan speed (500 lines per second), iris (6.0), gain (5.4) and offset (1.0). Background noise was reduced through Kalman filtering, whereby the image was scanned six times.

A small amount of coated particles was dispersed in immersion oil (Merck, Germany) (refractive index: 1.515) on a cover glass. The objective lens, located below the sample, was covered with immersion oil and was allowed to approach the bottom of the cover glass, until the sample was in focus. Images were exclusively recorded in the equatorial optical slice of the microparticle. Through the selection of appropriate CLSM settings, as defined above, it was assured that the image was neither undersaturated nor oversaturated, as this would lead to values for coating thickness that were too high or too low, respectively, with respect to reality. Using the 40× magnification lens, the confocal image covers an area of 285 × 285 μm^2. As digital image files in 1024 × 1024 pixel resolution were recorded, the image resolvable area (pixel) was about 0.278 × 0.278 μm^2, close to the resolution of the optics. If a Nyquist criterion is used, the resolution of the image is theoretically limited to 0.7 μm. An example of a typical CLSM image obtained is shown in Fig. 1, where the equatorial plane of a microparticle is visualized, recorded under both the epi-fluorescence and epi-reflectance mode. In the fluorescence mode, the coating, which is labelled with a fluorochrome (Rhodamine B), can be detected from the darker background as pixels with a grey value approaching 255 (white). In the reflectance mode, reflected laser light forms the image, so from Fig. 1 it can be observed that a material with a refractive index different from the core material was present around the glass bead. Based on this light scattering and from the comparison with the corresponding fluorescence image, it can be seen that coating regions showing a higher fluorescence contained more protein dry matter. This confirmed directly that the rhodamine was attached to the protein, and that the detected fluorescence was representative of the protein coating present. This finding supported the protocol used to derive microparticle coating thickness from CLSM images in the epi-fluorescence mode.

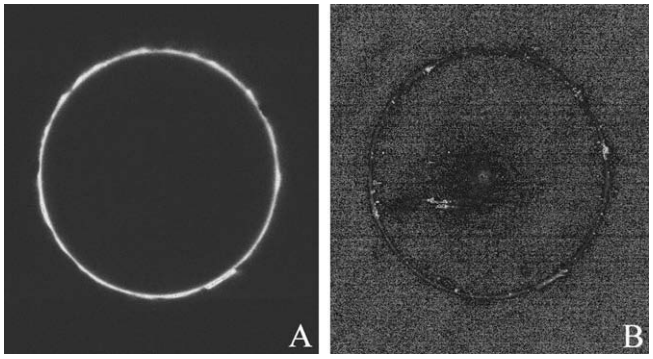

Fig. 1. Example of a typical CLSM microparticle image in the epi-fluorescence (A) and epi-reflectance (B) mode.

2.4. CLSM image analysis

Image analysis of the confocal recordings was performed using the software Image J 1.32j (National Institutes of Health, USA). An example of a raw image and its subsequent processing is given in Fig. 2. In order to improve the extraction of the information content of an image, reducing the background noise by Kalman filtering was a first step to reach the required contrast for discriminating between the fluorescent coating and the non-fluorescent environment. For measurements of feature-specific parameters related to object dimensions and shapes (in this case the two borders of the coating layer around the glass bead), the object of interest had to be segmented from the image [34]. First, the 8-bit colour image was converted into an 8-bit grey image, for which the grey value of each pixel is between 0 (black) and 255 (white). Segmentation of this grey image in order to distinguish the coating from its environment was performed by applying the automatic threshold function of Image J. The algorithm applied is similar to the Riddler and Calvard [35] optimal threshold method. After applying the Image J auto threshold, the image consisted of only two grey values: a black (grey value: 0) background (which contains both the glass bead core and the environment of the coated glass bead) and the white (grey value: 255) coating. In the resulting binary image, an oval was constructed around the coated particle and, from the oval centroid to the periphery, the sum of pixel grey values along a high number of radii was determined. As only contributions from pixels belonging to the coating are part of the sum of pixel intensities along each radius, the distribution of the radial sum around the oval is a direct indication of the coating thickness variation. Taking into account the grey value of a white pixel (255) and the conversion between distance in pixels and micrometer, the coating thickness distribution of a single microparticle was obtained. For the coated glass bead in Fig. 2, 120 radii were sampled, so 120 values of coating thickness were obtained. For all the beads investigated by CLSM in this study, samples were taken for every degree around the oval, so generating 360 values for microparticle coating thickness.

Generally, instead of obtaining one value for coating thickness, a distribution of coating thicknesses was obtained for every single microparticle. From this distribution, a number of parameters could be obtained for the microparticle coating considered: e.g., the average, as a measure of coating content; the standard deviation, as a measure of coating heterogeneity; the minimal recorded value, as a measure of the occurrence of imperfections. Distribution statistics calculations were performed using SPSS 10.0.1 (SPSS Inc., United States). As the aim of the study was to find whether coating thickness and coating quality differed between microparticles from different fluidized bed experiments, a number of microparticles from each experiment, representative of the bulk microparticle population, had to be investigated. In literature, contradictory figures are mentioned concerning the number of microparticles (from 15 to 1000) that need to be investigated to obtain a representative measure of microparticle characteristics [7,19,36–

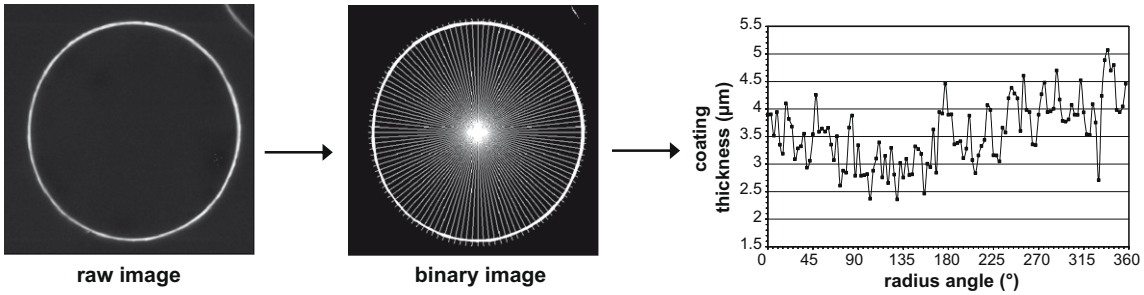

Fig. 2. CLSM image segmentation and further processing protocol.

38]. For this study, it was found that a population of 50 microparticles adequately represented the bulk microparticle population. Taking into account the number of observations (360) of coating thickness for each microparticle, a lumped dataset of 18,000 coating layer thickness observations was obtained for each experiment. In order to compare different experiments, the individually obtained values (from 50 coating thickness distributions for each experiment) for the mean and standard deviation of coating thickness, as well as the minimum coating thickness observed, were averaged over the random factor "particle". To estimate whether, e.g., average coating thickness differed significantly between different experiments, an adapted test for means comparison was used. This test assumes a mixed model with a random factor "particle" nested in a factor "experiment". The test statistic z is calculated as [39]

$$z = \left| \frac{\bar{\omega}_{(1)} - \bar{\omega}_{(2)}}{\sqrt{s^2_{(1)} + s^2_{(2)}}} \right| \tag{2}$$

$$\bar{\omega}_{(j)} = \frac{\hat{\omega}_{j1} + \hat{\omega}_{j2} + \cdots + \hat{\omega}_{jn_j}}{n_j} \quad (j : \text{experiment } 1, 2) \tag{3}$$

$$s^2_{(j)} = \frac{s^2_j}{n_j} + \frac{s^2_{j1} + s^2_{j2} + \cdots + s^2_{jn_j}}{n_j^2} \tag{4}$$

where $\hat{\omega}_{jn_j}$ is the average particle coating thickness value for each particle (n_j: 1, ..., 50), $s^2_{jn_j}$ is the estimator of the variance of $\hat{\omega}_{jn_j}$ and s^2_j is the sample variance of the n_j parameter estimations $\hat{\omega}_{jn_j}$ for one specific experiment. The standard deviations reported in the Results and discussion section correspond to the variance as calculated in Eq. (4). Using the central limit theorem, a similar explanation for the test statistic associated with the standard deviations of the coating thickness distributions of different experiments can be given, provided the distribution of the n_j values for the standard deviation of microparticles of a same experiment is chi-squared with (360−1) degrees of freedom. The resultant test statistics were compared with the threshold value of 1.96, corresponding to the 95% confidence level.

3. Results and discussion

3.1. Case-study 1: CLSM resolution and minimum coating layer thickness determination

In a first set of fluid bed experiments, a 5 wt% sodium caseinate solution labelled with Rhodamine B was sprayed downwards onto the fluidized glass beads. For all experiments, the position of the nozzle tip in the top-spray configuration was kept constant at 121 mm above the distributor. The liquid spray rate was 2.4 ± 0.1 g/min and the relative humidity of the inlet air was 53 ± 6%. The single parameter varying between the experiments of this test series was the amount of coating mass delivered to the powder bed, ranging from 1 to 3 wt% coating on core material.

In Table 1, for each experiment the reference values for the coating thickness (according to Eq. (1) and from the chemical protein determination data on 20 g of microparticles) are compared to the CLSM coating thickness distribution data of 50 microparticles.

In this work, coating quality is defined as the ratio of the average coating thickness, $d_{c,avg}$, to the average standard deviation of the coating thickness distributions, $d_{c,stdev}$. The higher this ratio, i.e., the thicker a coating of equal homogeneity is, or the more homogeneous the coating thickness distribution around a same average value is, the better the coating quality.

In Table 1, data on the core particle size of the 50 microparticles investigated by CLSM are also given. From this, it can be seen that the particle size of the samples did not significantly ($p > 0.05$) differ between experiments and hence, did not contribute to differences observed between different experiments.

From the CLSM coating thickness distribution data in Table 1, the mean coating thickness of all experiments, except for the coating levels of 1.0 wt% and 1.5 wt%, was found to be significantly different at a 95% confidence level. The effect of spraying a higher amount of coating material on the coating thickness heterogeneity, expressed as the standard deviation, was not clear from the data in Table 1. However, the coating quality was found to significantly increase with higher coating levels. Additionally, the minimum coating thickness values observed on individual microparticles increased for higher coating levels, while the extent to which locations of zero thickness prevailed on individual beads decreased for higher coating levels. For all experiments, however, coating deficiencies were encountered on the microparticles.

Table 1 also shows the comparison of the values of coating thickness, obtained using CLSM, with both the theoretical and experimental reference values. It can be concluded that the CLSM results were in good agreement with the two reference values from a coating level of 1.5–2.0 wt% onwards. For an average coating thickness below 1.5 µm, CLSM was found to overestimate the coating thickness. This can be explained by a decreasing contrast between the fluorescent thin coating layer and the non-fluorescent environment, when the coating thickness becomes smaller. For the selected confocal settings (such as laser power), a sharp delineation of the coating region, and hence proper thresholding, was not possible for coatings around 1 µm and thinner. As it was chosen to maintain these confocal settings throughout the work, this should be considered as the resolution limit of the confocal technique. This is close to the Nyquist criterion used for digital picture analysis with a pixel size of 0.285 µm.

Also, when comparing the reference values for coating thickness with the CLSM data, it needs to be taken into account that Eq. (1) assumes that all core particles have an equal size and assumes the exact knowledge of the coating material particle density. Also, the chemical protein determination is performed for about 20 g of

Table 1
Effect of the amount of sodium caseinate coating on glass beads: comparison of reference values for coating thickness (Eq. (1)) with CLSM coating thickness distribution data (d_c: coating thickness, d_p: core particle size).

Experiment	1.0 wt%	1.5 wt%	2.0 wt%	2.5 wt%	3.0 wt%
Reference values for coating thickness (Eq. (1))					
d_c, th (μm)	0.98	1.44	1.95	2.46	2.91
d_c, exp (μm)	1.16 ± 0.09^{a}	1.64 ± 0.23^{b}	2.17 ± 0.26^{c}	2.56 ± 0.20^{d}	2.92 ± 0.42^{d}
CLSM coating thickness distribution data of 50 individual microparticles/test					
d_c, avg (μm)	1.63 ± 0.08^{a}	1.84 ± 0.08^{a}	2.12 ± 0.08^{b}	2.58 ± 0.08^{c}	3.13 ± 0.09^{d}
d_c, stdev (μm)	0.54 ± 0.01^{ac}	0.55 ± 0.01^{ac}	0.52 ± 0.01^{ab}	0.50 ± 0.01^{b}	0.59 ± 0.02^{c}
d_c, min (μm)	0.01 ± 0.03	0.04 ± 0.08	0.39 ± 0.44	0.98 ± 0.58	1.32 ± 0.76
Coating quality	3.0 ± 0.2^{a}	3.3 ± 0.2^{a}	4.1 ± 0.2^{b}	5.2 ± 0.3^{c}	5.3 ± 0.3^{c}
d_p (μm)	225 ± 14^{a}	222 ± 14^{a}	226 ± 15^{a}	229 ± 17^{a}	227 ± 15^{a}

For each row, significantly different values ($p < 0.05$) are indicated with a different superscript letter.
Theory (th), experimental (exp), average (avg), standard deviation (stdev), minimum (min).

microparticles, implying millions of individual particles. Coating thickness distribution analysis by CLSM, however, allows an individual particle to be examined.

3.2. Case-study 2: effect of fluidized bed process settings on coating quality

In a second fluid bed test series, the influence of the spray nozzle position relative to the powder bed on the coating thickness and coating quality was investigated using two different proteins, sodium caseinate and gelatine hydrolysate, as the coating material. In all experiments, 200 g of a 10 wt% protein solution was atomized onto the fluidized glass beads. The distance between the nozzle tip and the fluidized core particles was minimal in the case of the bottom-spray experiment, where the partition height was set at 10 mm. The distance between the distributor and the nozzle tip was gradually increased in the experiments in the top-spray configuration: 121 mm in the "top low" experiment, 168 mm in the "top middle" experiment and 270 mm in the "top high" experiment. It is important to emphasize that the powder bed height in all three top-spray configuration experiments was kept constant as defined by the selected air flow rate. From previous research [40], it was found that for the selected conditions of the top-spray fluidized bed experiments, the particle bed height was 120 mm (relative to the distributor), implying that in the "top low" experiment, the nozzle was almost submerged in the powder bed. In all experiments with the sodium caseinate coating solution, the relative humidity of the inlet air was 64 ± 3% and the liquid spray rate was 5.2 ± 0.1 g/min. These parameters were 52 ± 6% and 4.9 ± 0.1 g/min, respectively, for the experiments with the gelatine hydrolysate coating solution.

In Table 2, the experimental reference value for the coating thickness of the different experiments is compared to the CLSM coating thickness distribution data of 50 microparticles for the experiment with sodium caseinate as coating material.

Despite the large differences involved in their determination, the average values of the coating thickness of the different experiments as obtained by CLSM were in good agreement with the respective experimental reference values. It could be clearly demonstrated that the average coating thickness decreased with increasing distance between the nozzle tip and the powder bed (from bottom-spray to top-spray with the nozzle in the "high" position). Also, it was found that the coating thickness heterogeneity (standard deviation of the coating thickness distribution) significantly ($p < 0.05$) increased from the bottom-spray experiment to the top-spray "high" experiment, i.e., from the shortest to the longest average droplet travel distance. Intermediate values for coating thickness heterogeneity were obtained for the top-spray "low" and top-spray "middle" experiments, which were not found to be significantly ($p > 0.05$) different for this quality parameter. When combining the results for average coating thickness and coating heterogeneity, coating quality was found to significantly ($p < 0.05$) decrease with increasing distance between the nozzle tip and the powder bed. A significantly better coating quality was obtained for the bottom-spray experiment, compared to all three top-spray experiments. This is in line with the reported better coating quality of a well designed bottom-spray fluid bed process compared to a similar process in the top-spray configuration [28]. The coating quality of the top-spray experiment with the nozzle in the highest position was significantly ($p < 0.05$) lower compared to the top-spray experiments with the nozzle in a lower position, i.e., very close to the powder bed. These findings can be attributed to spray-drying of the coating solution droplets which is more pronounced with increasing distance the droplets have to travel before impinging onto the core particles. This does result not only in lower amounts of coating retrieved on the core parti-

Table 2
Influence of the spray nozzle position when spraying a sodium caseinate coating on glass beads: comparison of the experimental reference values for coating thickness (Eq. (1)) with CLSM coating thickness distribution data (d_c: coating thickness, d_p: core particle size).

Experiment	Bottom	Top low	Top middle	Top high
Reference values for coating thickness (Eq. (1))				
d_c, exp (μm)	2.42 ± 0.04^{a}	2.37 ± 0.06^{a}	2.19 ± 0.10^{b}	1.66 ± 0.04^{c}
CLSM coating thickness distribution data of 50 individual microparticles/test				
d_c, avg (μm)	2.64 ± 0.10^{a}	2.59 ± 0.12^{a}	2.37 ± 0.13^{a}	1.76 ± 0.22^{b}
d_c, stdev (μm)	0.61 ± 0.02^{a}	0.81 ± 0.03^{b}	0.86 ± 0.03^{b}	1.55 ± 0.09^{c}
d_c, min (μm)	0.86 ± 0.51	0.19 ± 0.29	0.05 ± 0.14	0
Coating quality	4.3 ± 0.3^{a}	3.2 ± 0.3^{b}	2.8 ± 0.2^{b}	1.1 ± 0.2^{c}
d_p (μm)	202 ± 21^{a}	208 ± 22^{a}	211 ± 22^{a}	206 ± 25^{a}

For each row, significantly different values ($p < 0.05$) are indicated with a different superscript letter.
Experimental (exp), average (avg), standard deviation (stdev), minimum (min).

cles, as part of the spray-dried coating will be entrained with the fluidization air and will be collected in the exhaust filter, but also in a lower coating quality. Upon eventual contact with cores, spray-dried coating material does not wet the surface nor does it uniformly spread out. Moreover, with increasing distance between the nozzle tip and the powder bed, more core material remained uncoated and lower average values for the minimum coating thickness were found. Ultimately, for the top-spray experiment with the nozzle in the highest position, on all beads coating deficiencies (zero coating thickness locations) were observed.

In addition to the CLSM results described in Table 2, Fig. 3 shows SEM images of the microparticles of each experiment at three levels of magnification. From SEM analysis, it can be qualitatively confirmed that the coating quality was superior for the bottom-spray experiment and worsened with increasing distance between the top-spray nozzle tip and the powder bed. For the bottom-spray experiment, a dense homogeneous coating was observed. In contrast, for the microparticles of the top-spray coating experiments, more coating deficiencies were detected. While a relatively good coating was still obtained when the top-spray nozzle was in the "low" position, a bad coating showing deep craters and high amounts of incorporated spray-dried material was observed when the top-spray nozzle was in the "high" position.

Based on the amount of coating material applied, the experiment with the nozzle in the "low" position in Table 2 can be compared with the two experiments with the highest coating level (2.5–3 wt%) of the first fluid bed test series (Table 1). The experiment in the second fluid bed test series (Table 2, "top low") resulted in a significantly ($p < 0.05$) lower coating quality compared to the experiments (2.5–3 wt%) from Table 1. This may be explained by the fact that in the second test series, a more concentrated sodium caseinate solution was sprayed at a higher spray rate, compared to the experiments of the first test series. As a result, the coating droplets may have spread out less due to a higher viscosity, which implies a lower coating quality.

3.3. Case-study 3: effect of coating material on coating quality

For gelatine hydrolysate as a coating material, Table 3 shows the CLSM coating thickness distribution data of 50 microparticles of the different experiments of the second fluid bed test series, compared to their respective experimental reference value for the coating thickness.

Comparable to the findings for sodium caseinate, the CLSM results for average thickness of the gelatin hydrolysate coating layers were in good agreement with the experimental reference values. Also, for the experiments with the nozzle in the top-spray configuration, spray-drying of the coating solution was found to be more pronounced with increasing distance between the nozzle tip and the powder bed: the amount of coating material retrieved on the microparticle surface decreased from the experiment with the top-spray nozzle in the "low" position to the one with the nozzle in the "high" position. With respect to the coating thickness heterogeneity, given by the average standard deviation of the coating thickness distributions in Table 3, generally more homogeneous coatings were obtained for the top-spray experiments compared to the bottom-spray experiment. Together with equal values of average coating thickness, this resulted in a significantly ($p < 0.05$) better coating quality for the "top low" experiment compared to the bottom-spray

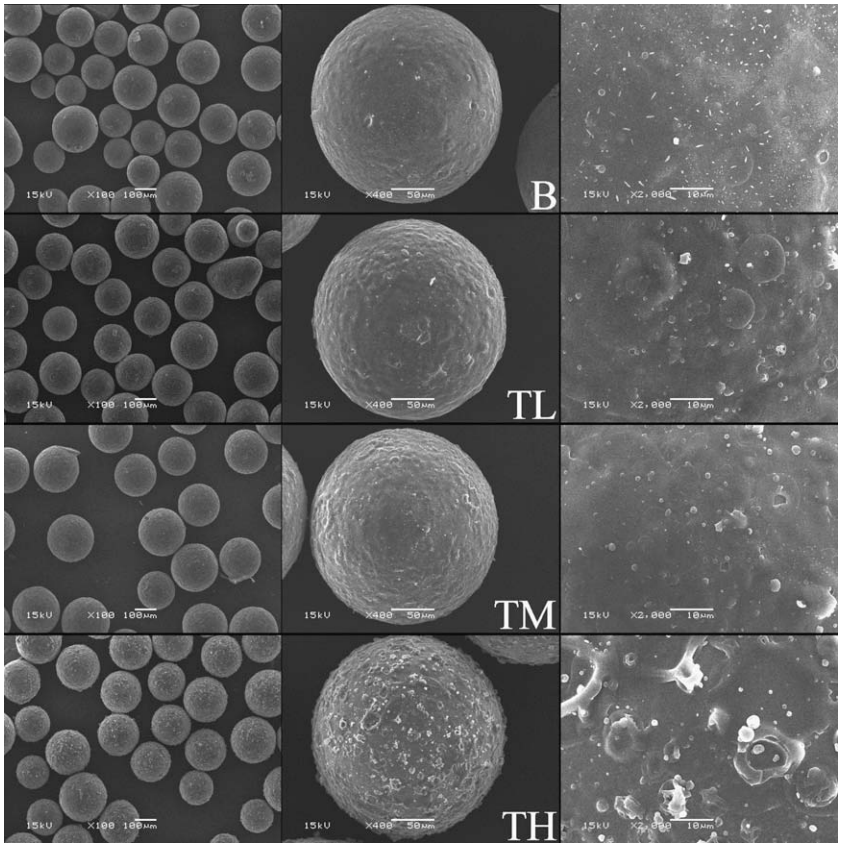

Fig. 3. SEM images of sodium caseinate coated microparticles: influence of the spray nozzle position (B: bottom, TL: top low, TM: top middle, TH: top high) (magnification from left to right: 100×, 400× and 2000×).

Table 3
Influence of the spray nozzle position when spraying a gelatine hydrolysate coating on glass beads: comparison of the experimental reference values for coating thickness (Eq. (1)) with CLSM coating thickness distribution data (d_c: coating thickness, d_p: core particle size).

Experiment	Bottom	Top low	Top middle	Top high
Reference values for coating thickness (Eq. (1))				
d_c, exp (μm)	2.03 ± 0.03^{a}	1.98 ± 0.06^{b}	1.83 ± 0.04^{c}	1.24 ± 0.03^{d}
CLSM coating thickness distribution data of 50 individual microparticles/test				
d_c, avg (μm)	2.05 ± 0.17^{a}	2.09 ± 0.14^{a}	1.79 ± 0.13^{a}	1.36 ± 0.15^{b}
d_c, stdev (μm)	1.18 ± 0.07^{a}	0.95 ± 0.04^{bc}	0.87 ± 0.02^{b}	1.00 ± 0.03^{c}
d_c, min (μm)	0	0	0	0
Coating quality	1.7 ± 0.2^{a}	2.2 ± 0.2^{b}	2.1 ± 0.2^{ab}	1.4 ± 0.2^{c}
d_p (μm)	208 ± 20^{a}	203 ± 21^{a}	221 ± 16^{a}	212 ± 19^{a}

For each row, significantly different values ($p < 0.05$) are indicated with a different superscript letter.
Experimental (exp), average (avg), standard deviation (stdev), minimum (min).

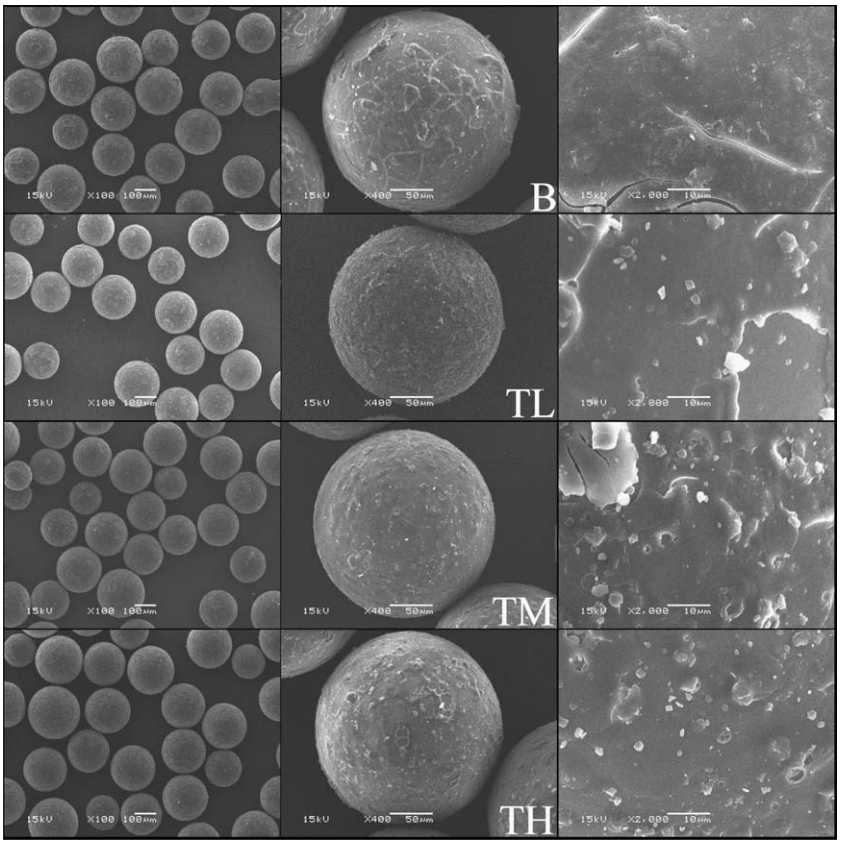

Fig. 4. SEM images of gelatine hydrolysate coated microparticles: influence of the spray nozzle position (B: bottom, TL: top low, TM: top middle, TH: top high) (magnification from left to right: 100×, 400× and 2000×).

experiment. Also, the coating thickness heterogeneity of the microparticles from the "top high" experiment was found to be lower for the gelatine hydrolysate coating compared to the sodium caseinate coating. The SEM images in Fig. 4 demonstrate that in the three top-spray experiments, holes and incorporated spray-dried material are present, but to a lesser extent for the "top high" experiment when compared to the respective sodium caseinate coating in Fig. 3.

This fluidized bed coating experiment with gelatine hydrolysate did not confirm the general acceptance of a superior coating quality of a bottom-spray fluid bed coating process compared to a top-spray process [28]. This may be explained by the higher viscosity and tackiness of gelatine hydrolysate compared to sodium caseinate. As for the bottom-spray process, overall the distance between the nozzle tip and the particles will be smaller than for a top-spray process, the particles will be more excessively wetted which, combined with a higher viscosity of the coating liquid, may impart proper spreading. Another problem typically observed with gelatine hydrolysate is the presence of cracks (Fig. 4). As the gelatine is hydrolysed, less molecular interaction is possible and a more brittle coating is obtained. During fluidization processes, the coated microparticles are subjected to particle–particle and particle–wall contacts, which may have resulted in cracks in this type of coating material [41].

4. Conclusions

Confocal laser scanning microscopy (CLSM) was found to be an adequate non-destructive technique for the quantification of the coating thickness and coating quality of thin-coated (<5 μm) small

(200 μm) inert spherical particles. A CLSM protocol was developed which allowed, in combination with image analysis, to quantify the microparticle coating quality with high accuracy.

Compared to other techniques, where a single value for coating thickness as an average for the whole sample population is obtained, the CLSM protocol generates a coating thickness distribution for each individual microparticle. It is clear that in this distribution, much more information such as coating thickness heterogeneity and coating deficiencies is contained.

In a number of case-studies performed in the fluidized bed, the feasibility of using the CLSM protocol developed to quantify coating thickness and coating quality was demonstrated. Good agreement between the CLSM results and the reference values for coating thickness was seen for values of coating thickness down to 1–1.5 μm. Furthermore, it could be quantified through CLSM to which extent process settings (increased distance between the nozzle tip and the core particle bed; a more concentrated coating solution) led to a decrease in the quality of the coating layer. Also the differences in coating quality when different coating materials were used, could be quantified. Moreover, all these CLSM findings could be qualitatively confirmed from SEM images.

In order to enhance the applicability of the developed CLSM methodology in the study of microparticle coating quality, efforts are under-way to adapt the image analysis protocol to non-spherical and porous particles.

Acknowledgements

The authors gratefully acknowledge the financial support from the Fund for Scientific Research – Flanders (Belgium) (F.W.O.-Vlaanderen).

References

[1] F. Shahidi, X.Q. Han, Encapsulation of food ingredients, Crit. Rev. Food Sci. Nutr. 33 (6) (1993) 501–547.
[2] F. Depypere, K. Dewettinck, F. Ronsse, J.G. Pieters, Food powder microencapsulation: principles, problems and opportunities, Appl. Biotechnol. Food Sci. Policy 1 (2) (2003) 75–94.
[3] M. Andersson, M. Josefson, F.W. Langkilde, K.G. Wahlund, Monitoring of a film coating process for tablets using near infrared reflectance spectroscopy, J. Pharmaceut. Biomed. Anal. 20 (1–2) (1999) 27–37.
[4] J.D. Kirsch, J.K. Drennen, Determination of film-coated tablet parameters by near-infrared spectroscopy, J. Pharmaceut. Biomed. Anal. 13 (10) (1995) 1273–1281.
[5] R. Wesdyk, Y.M. Joshi, N.B. Jain, K. Morris, A. Newman, The effect of size and mass on the film thickness of beads coated in fluidized bed equipment, Int. J. Pharmaceut. 65 (1–2) (1990) 69–76.
[6] M. Andersson, B. Holmquist, J. Lindquist, O. Nilsson, K.G. Wahlund, Analysis of film coating thickness and surface area of pharmaceutical pellets using fluorescence microscopy and image analysis, J. Pharmaceut. Biomed. Anal. 22 (2) (2000) 325–339.
[7] C.C. Larsen, J.M. Sonnergaard, P. Bertelsen, P. Holm, Validation of an image analysis method for estimating coating thickness on pellets, Eur. J. Pharmaceut. Sci. 18 (2) (2003) 191–196.
[8] A. Lamprecht, U. Schäfer, C.M. Lehr, Structural analysis of microparticles by confocal laser scanning microscopy, AAPS Pharmaceut. Sci. Tech. 1 (3) (2000) article 17.
[9] G. Binnig, C.F. Quate, C. Gerber, Atomic force microscope, Phys. Rev. Lett. 56 (9) (1986) 930–933.
[10] M. Kaláb, P. Allan-Wojtas, S.S. Miller, Microscopy and other imaging techniques in food structure analysis, Trends Food Sci. Technol. 6 (6) (1995) 177–186.
[11] A. Ringqvist, L.S. Taylor, K. Ekelund, G. Ragnarsson, S. Engström, A. Axelsson, Atomic force microscopy analysis and confocal Raman microimaging of coated pellets, Int. J. Pharmaceut. 267 (1-2) (2003) 35–47.
[12] J. Ubbink, P. Schär-Zammaretti, Probing bacterial interactions: integrated approaches combining atomic force microscopy electron, microscopy and biophysical techniques, Micron 36 (4) (2005) 293–320.
[13] M.D. Mowery, R. Sing, J. Kirsch, A. Razaghi, S. Béchard, R.A. Reed, Rapid at-line analysis of coating thickness and uniformity on tablets using laser-induced breakdown spectroscopy, J. Pharmaceut. Biomed. Anal. 28 (5) (2002) 935–943.
[14] Y. Mouget, P. Gosselin, M. Tourigny, S. Béchard, Three-dimensional analyses of tablet content and film coating uniformity by laser-induced breakdown spectroscopy (LIBS), Am. Lab. 35 (4) (2003) 20–22.
[15] M. Ruotsalainen, J. Heinämäki, H. Guo, N. Laitinen, J. Yliruusi, A novel technique for imaging film coating defects in the film–core interface and surface of coated tablets, Eur. J. Pharmaceut. Biopharmaceut. 56 (3) (2003) 381–388.
[16] B.L. Strand, Y.A. Mørch, T. Espevik, G. Skjåk-Bræk, Visualization of alginate-poly-l-lysine-alginate microcapsules by confocal laser scanning microscopy, Biotechnol. Bioeng. 82 (4) (2003) 386–394.
[17] G.M.R. Vandenbossche, P. Van Oostveldt, J.P. Remon, A fluorescent method for the determination of the molecular weight cut-off of alginate–polylysine microcapsules, J. Pharmaceut. Pharmacol. 43 (4) (1991) 275–277.
[18] A. Lamprecht, U. Schäfer, C.M. Lehr, Visualization and quantification of polymer distribution in microcapsules by confocal laser scanning microscopy, Int. J. Pharmaceut. 196 (2) (2000) 223–226.
[19] A. Lamprecht, U. Schäfer, C.M. Lehr, Characterization of microcapsules by confocal laser scanning microscopy: structure, capsule wall composition and encapsulation rate, Eur. J. Pharmaceut. Biopharmaceut. 49 (1) (2000) 1–9.
[20] H. Zimmermann, M. Hillgärtner, B. Manz, P. Feilen, F. Brunnenmeier, U. Leinfelder, M. Weber, H. Cramer, S. Schneider, C. Hendrich, F. Volke, U. Zimmermann, Fabrication of homogeneously cross-linked, functional alginate microcapsules validated by NMR-, CLSM- and AFM-imaging, Biomaterials 24 (12) (2003) 2083–2096.
[21] C.Y. Gao, S. Leporatti, S. Moya, E. Donath, H. Mohwald, Swelling and shrinking of polyelectrolyte microcapsules in response to changes in temperature and ionic strength, Chem. Eur. J. 9 (4) (2003) 915–920.
[22] L.Q. Ge, H. Möhwald, J.B. Li, Polymer-stabilized phospholipids vesicles formed on polyelectrolyte multilayer capsules, Biochem. Biophys. Res. Commun. 303 (2) (2003) 653–659.
[23] O.I. Vinogradova, Mechanical properties of polyelectrolyte multilayer microcapsules, J. Phys. Condens. Matter 16 (32) (2004) R1105–R1134.
[24] F. Depypere, J.G. Pieters, K. Dewettinck, CFD analysis of air distribution in fluidised bed equipment, Powder Technol. 145 (3) (2004) 176–189.
[25] F. Depypere, J.G. Pieters, K. Dewettinck, Expanded bed height determination in a tapered fluidised bed reactor, J. Food Eng. 67 (3) (2005) 353–359.
[26] D.E. Wurster, Air suspension technique of coating drug particles a preliminary report, J. Am. Pharmaceut. Assoc. (Baltim) 48 (8) (1959) 451–454.
[27] L.S. Jackson, K. Lee, Microencapsulation and the food industry, Lebensmittel-Wissenschaft und – Technologie – Food Sci. Technol. 24 (4) (1991) 289–297.
[28] D. Jones, Air suspension coating for multiparticulates, Drug Dev. Ind. Pharm. 20 (20) (1994) 3175–3206.
[29] F.N. Christensen, P. Bertelsen, Qualitative description of the Wurster-based fluid-bed coating process, Drug Dev. Ind. Pharm. 23 (5) (1997) 451–463.
[30] K. Dewettinck, L. Deroo, W. Messens, A. Huyghebaert, Agglomeration tendency during top-spray fluidized bed coating with gums, Lebensmittel-Wissenschaft und – Technologie – Food Sci. Technol. 31 (6) (1998) 576–584.
[31] O.H. Lowry, N.J. Rosebrough, A.L. Farr, R.J. Randall, Protein measurement with the Folin phenol reagent, J. Biol. Chem. 193 (1) (1951) 265–275.
[32] G.L. Miller, Protein determination for large number of samples, Anal. Chem. 31 (5) (1959) 964.
[33] G.R. Schacterle, R.L. Pollack, A simplified method for the quantitative assay of small amounts of protein in biologic material, Anal. Chem. 51 (2) (1973) 654–655.
[34] M. Ferrando, W.E.L. Spiess, Review: confocal scanning laser microscopy. A powerful tool in food science, Food Sci. Technol. Int. 6 (4) (2000) 267–284.
[35] T.W. Riddler, S. Calvard, Picture thresholding using an iterative selection method, IEEE Trans. Syst. Man Cybernetics SMC-8 (1978) 630–632.
[36] L. Hellen, J. Yliruusi, E. Kristoffersson, Process variables of instant granulator and spheronizer . Part 2. Size and size distribution of pellets, Int. J. Pharmaceut. 96 (1–3) (1993) 205–216.
[37] H. Lindner, P. Kleinebudde, Characterization of pellets by means of automatic image analysis, Pharmaceut. Ind. 55 (7) (1993) 694–701.
[38] F. Podczeck, S.R. Rahman, J.M. Newton, Evaluation of a standardised procedure to assess the shape of pellets using image analysis, Int. J. Pharmaceut. 192 (2) (1999) 123–138.
[39] I. Foubert, P.A. Vanrolleghem, K. Dewettinck, A differential scanning calorimetry method to determine the isothermal crystallization kinetics of cocoa butter, Thermochim. Acta 400 (1–2) (2003) 131–142.
[40] F. Depypere, J.G. Pieters, K. Dewettinck, PEPT visualisation of particle motion in a tapered fluidised bed coater, J. Food Eng. 93 (3) (2009) 324–336.
[41] K. Dewettinck, W. Messens, L. Deroo, A. Huyghebaert, Agglomeration tendency during top-spray fluidized bed coating with gelatine and starch hydrolysate, Lebensmittel-Wissenschaft und – Technologie – Food Sci. Technol. 32 (2) (1999) 102–106.